Separation Science and Technology

ISSN: 0149-6395 (Print) 1520-5754 (Online) Journal homepage: https://www.tandfonline.com/loi/lsst20

Permeate-Flux Declination for Ultrafiltration along Membrane Tubes

H. M. Yeh , Z. Y. Lin & C. H. Li

To cite this article: H. M. Yeh , Z. Y. Lin & C. H. Li (2010) Permeate-Flux Declination for Ultrafiltration along Membrane Tubes, Separation Science and Technology, 45:14, 1995-2003, DOI: 10.1080/01496395.2010.504429

To link to this article: https://doi.org/10.1080/01496395.2010.504429

Published online: 15 Sep 2010.

Separation Science and Technology, 45: 1995–2003, 2010

ISSN: 0149-6395 print/1520-5754 online
DOI: 10.1080/01496395.2010.504429

Taylor & Francis
Taylor & Francis Group

Permeate-Flux Declination for Ultrafiltration along Membrane Tubes

H. M. Yeh, Z. Y. Lin, and C. H. Li
Department of Chemical and Materials Engineering, Tamkang University, Tamsui, Taipei County, Taiwan

The correlation equations for predicting local permeate fluxes in tubular-membrane ultrafilters were derived from mass and momentum balances by the modified resistance-in-series model with the considerations of the increment of concentration polarization and the declines of transmembrane pressure and flow rate, along the membrane tube. Ultrafiltration of dextran T500 aqueous solution in a tubular microporous ceramic module has been carried out under various feed concentrations, transmembrane pressures, and feed flow rates, and many experimental data of ten-point local permeate fluxes along the tube were obtained to confirm the correlation predictions. The increment of concentration polarization, as well as the decline of permeate flux, along the tube was also discussed.

Keywords concentration polarizationx; membrane tube; permeate flux; ultrafiltration

INTRODUCTION

Ultrafiltration membrane process has now become an increasingly important industrial process for the concentration, purification, or dewatering of macromolecular and colloidal species in solution; it is usually used in the food, beverage, and dairy industries, for effluent treatment, and biotechnology and medical applications (1–3). The advantage of ultrafiltration as compared to conventional dewatering processes, such as evaporation, freeze concentration, or freeze drying, is the absence of a change in phase or state of the solvent during dewatering process, resulting in considerable savings in energy.

Ultrafiltration is primarily a size-exclusion-based, pressure-driven membrane separation process; the pressure applied to the working fluid provides the potential to force the solvent to flow through the membrane. During operation, the solute is transported to the membrane surface by the convective flow of the permeant; this is balanced by diffusion back to the bulk. In cross-flow ultrafiltration the permeate flux generally declines along the flow direction due to the phenomenon of concentration polarization by the rejected particles, which is a common feature of all pressure-driven membrane processes (4). Several hydraulic approaches developed for reducing the effect of concentration polarization to enhance the permeate flux, has been discussed thoroughly (5–17). The use of inserts, such as metal grills (7), static rods (8), spiral wire (9), disc, and doughnut shape inserts (10) and helical baffles (11–13), in a tubular membrane have been tried to different membrane processes. Da Costa and coworkers performed an extensive study of ultrafiltration flux by net-type spacers (14–17). The applications of inserting solid and wired rods in the tubular membrane systems were also reported (5,6).

A number of mathematical models are available in the literature that attempt to describe the mechanism of transport through membranes. In the gel polarization model, the permeate flux is reduced by hydraulic resistance of the gel layer (18). In the osmotic pressure model, the permeate flux reduction results in effective transmembrane pressure that occurs as osmotic pressure of the retentate increases (19). In the resistance-in-series model, the permeate flux decreases due to the resistance caused by fouling or solute adsorption and concentration polarization. This last method easily describes the relationships of the permeate flux with the operating parameters (20–26). Chhatre and Marathe reported that the experimental values of permeate flux for the removal of Ni from aqueous phase by using sodium dodecycle sulphate for micellization, were in close agreement with the predicted values obtained by the resistance in the series model (20). It was also pointed out that this model is particularly applicable for the analysis of flux decline in ultrafiltration (21–24). In this study, we ultrafiltered the macromolecular solution in a tubular membrane module and measured the permeate fluxes along the tube under various operating conditions. The declines of the permeate flux was also analyzed by mass and momentum balances coupled with the use of the modified resistance-in-series model.

Received 9 October 2008; accepted 4 April 2010.
Address correspondence to H. M. Yeh, Department of Chemical Engineering, Tamkang University, Tamsui, Taipei 251, Taiwan. Tel.: +886-2-2621-5656/ext.2601; Fax: +886-2-26209887. E-mail: hmyeh@mail.tku.edu.tw

THEORY

Resistance-in-Series Model

Although the osmotic pressure at the membrane surface also affects the permeate flux, ultrafiltration usually deals with the separation of fairly large molecules and the osmotic pressures involved in ultrafiltration processes are fairly low and negligible. Accordingly, the permeate flux J(z) for ultrafiltration in the resistance-in-series model, permeate flux J(z) may be expressed as

$$J(z) = \frac{\Delta P(z)}{R_m + R_f + R_p} \tag{1}$$

where R_m denotes the intrinsic resistance, and R_p and R_f are the resistances due to the concentration/gel layer and those due to other fouling phenomena such as adsorption, respectively, while $\Delta P(z)$ is the transmembrane pressure defined as

$$\Delta P(z) = P(z) - P_s \tag{2}$$

In the above equation, P(z) is the pressure distribution of the tube side along the axial direction z, and P_s is the permeate pressure of the shell side which may be assumed to be constant.

As mentioned before, the concentration polarization is a common feature of all pressure-driven membrane processes. It is dependent on the operating parameter such as pressure, temperature, feed concentration, and velocity, and increases along the membrane tube. Accordingly, we may assume that for constant operating temperature

$$R_p = \beta(z)\Delta P(z) \tag{3}$$

where the proportional factor $\beta(z)$ may be simply assumed to be linearly increasing along the tube, i.e.,

$$\beta(z) = \beta_i[1 + \alpha(z/L)] \tag{4}$$

and β_i is the value of β at the inlet and α is a constant; both are to be determined experimentally. Thus, Eq. (3) may be rewritten as

$$R_p = \beta_i[1 + \alpha(z/L)]\Delta P(z) \tag{5}$$

Substitution of Eq. (5) into Eq. (1) yields

$$J(z) = \frac{\Delta P(z)}{R_m + R_f + \beta_i[1 + \alpha(z/L)]\Delta P(z)} \tag{6}$$

Mass Balance

Figure 1 shows a microporous membrane tube of radius r_m and length L installed in the experimental apparatus.

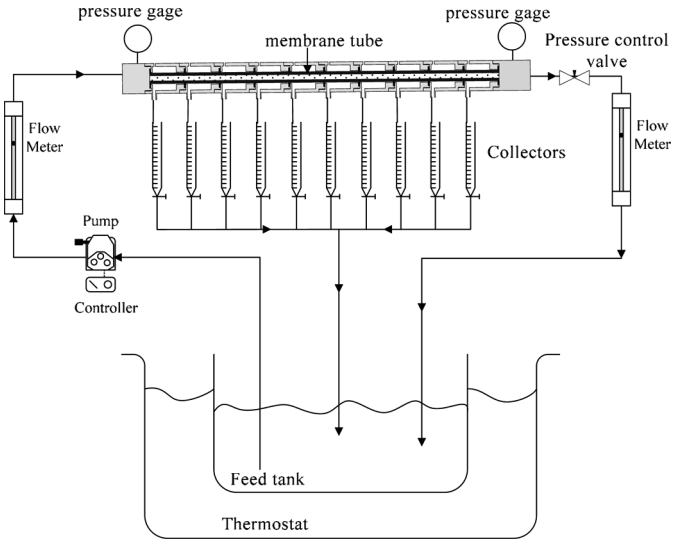

FIG. 1. Experimental apparatus.

Let Q(z) be the volume flow rate of the feed solution in a microporous membrane tube, a mass balance over a slice of dz of the tube gives

$$\frac{dQ}{dz} = -2\pi r_m J(z) \tag{7}$$

Integrating Eq. (7) from the inlet ($z = 0$, $Q = Q_i$) to the outlet ($z = L$, $Q = Q_o$) of the tube, one has

$$Q_o = Q_i - 2\pi r_m L\bar{J} \tag{8}$$

where $\bar{J}$ is the average value of J(z) defined as

$$\bar{J} = \frac{1}{L}\int_0^L J(z)dz \tag{9}$$

Momentum Balance

Since the permeation rate of membrane ultrafiltration is very small compared with the volume flow rate in a membrane tube, it can be assumed that the local decline in hydraulic pressure within the membrane tube is simply given by the Hagen-Poiseuille equation in terms of the average volume flow rate $\bar{Q}$ (5)

$$\frac{dP}{dz} = -\frac{8\mu\bar{Q}}{\pi r_m^4} \tag{10}$$

where

$$\bar{Q} = \frac{Q_i + Q_o}{2} = Q_i - \pi r_m L\bar{J} \tag{11}$$

Integration of Eq. (10) with the use of boundary condition: $P = P_i$ at $z = 0$, results in

$$P(\xi) = P_i - \left(\frac{8\mu\overline{Q}L}{\pi r_m^4}\right)\xi \tag{12}$$

where

$$\xi = \frac{z}{L} \tag{13}$$

and the transmembrane pressure is obtained by substituting Eqs. (11) and (12) into Eq. (2). The result is

$$\Delta P(\xi) = \Delta P_i - (mQ_i - n\bar{J})\xi \tag{14}$$

where

$$\Delta P_i = P_i - P_s \tag{15}$$

$$m = \frac{8\mu L}{\pi r_m^4} \tag{16}$$

$$n = \frac{8\mu L^2}{r_m^3} \tag{17}$$

and the transmembrane pressure at the outlet of a membrane tube is

$$\Delta P_o = \Delta P_i - (mQ_i - n\bar{J}) \tag{18}$$

Permeate Flux

Substitution of Eq. (14) into Eq. (6) yields the expression for local permeate flux in a microporous membrane tube

$$J(\xi) = \frac{\Delta P_i - (mQ_i - n\bar{J})\xi}{R_m + R_f + \beta_i(1 + \alpha\xi)[\Delta P_i - (mQ_i - n\bar{J})\xi]} \tag{19}$$

The average permeate flux can be obtained by substituting Eq. (19) into Eq. (9)

$$\bar{J} = \int_0^1 J(\xi)d\xi \tag{20}$$

$$= \int_0^1 \frac{-\Delta P_i\, d\xi}{A\xi^2 + B\xi + C} + \int_0^1 \frac{(mQ_i - n\bar{J})\xi\, d\xi}{A\xi^2 + B\xi + C} \tag{21}$$

where

$$A = (mQ_i - n\bar{J})\beta_i\alpha \tag{22}$$

$$B = [(mQ_i - n\bar{J}) - \alpha\Delta P_i]\beta_i \tag{23}$$

$$C = -(R_m + R_f + \beta_i\Delta P_i) \tag{24}$$

After integration, Eq. (21) becomes

$$\begin{aligned}\bar{J} &= \int_0^1 \frac{-\Delta P_i\, d\xi}{A\xi^2 + B\xi + C} + \left[\frac{(mQ_i - n\bar{J})}{2A}\ln\left|\frac{A + B + C}{C}\right|\right. \\ &\quad \left. - \frac{(mQ_i - n\bar{J})B}{2A}\int_0^1 \frac{d\xi}{A\xi^2 + B\xi + C}\right] \\ &= -\left[\Delta P_i + \frac{(mQ_i - n\bar{J})B}{2A}\right]\int_0^1 \frac{d\xi}{A\xi^2 + B\xi + C} \\ &\quad + \frac{(mQ_i - n\bar{J})}{2A}\ln\left|\frac{A + B + C}{C}\right|\end{aligned} \tag{25}$$

where

$$\int_0^1 \frac{d\xi}{A\xi^2 + B\xi + C} = \frac{1}{\sqrt{B^2 - 4AC}} \times \ln\left|\frac{(2A + B - \sqrt{B^2 - 4AC})(B + \sqrt{B^2 - 4AC})}{(2A + B + \sqrt{B^2 - 4AC})(B - \sqrt{B^2 - 4AC})}\right| \text{ if } B^2 > 4AC \tag{26}$$

$$= \frac{2}{\sqrt{4AC - B^2}}\left[\tan^{-1}\frac{2A + B}{\sqrt{4AC - B^2}} - \tan^{-1}\frac{B}{\sqrt{4AC - B^2}}\right], \quad \text{if } B^2 < 4AC \tag{27}$$

EXPERIMENTAL

Apparatus and Materials

The experimental apparatus used in this work is shown in Fig. 1. The membrane medium used was mainly 40 kDa MWCO tubular ceramic membrane (Carbsep, length $L = 0.4$ m, inside diameter $2r_m = 6 \times 10^{-3}$ m). The tested solute was dextran T500 (Pharmacia Co.). The solvent was distillated water. The feed solution was circulated by a high-pressure pump with a variable feed motor (L-07553-20, Cole-Parmer Co.), the liquid flow rate was observed by a flowmeter (IR-OPFLOW 502-111, Headland Co.). The feed pressure was controlled by using an adjusting valve at the outlet of the tubular-membrane module, and the gauge pressures at the tubular inlet (P_i), the outlet (P_o) and at the shell side (P_p) were measured with pressure transmitters (Model 891, 14, 425, Wika Co.). There were ten outlets on the shell side along the flow direction for measuring the local permeate fluxes at $z = 2$, 6, 10, 14, 18, 22, 26, 30, 34, and 38 cm.

Experimental Conditions and Procedures

The experimental conditions were as follows: Feed concentration C_i: 0.1, 0.5, 1.0 wt%; Feed flow rate $Q_i \times 10^6 =$ 1.67, 2.50, 3.33, 4.17 m^3/s; $u_i = Q_i/\pi\ r_m^2 = 0.059$, 0.08, 0.118, 0.147 m/s; Feed transmembrane pressure ΔP_i: 30, 50, 80, 110, 140 kPa.

TABLE 1
Experimental data of permeate flux for pure water with $u_i = 0.147\ m/s$

$\Delta P_i \times 10^{-5}$ (Pa)	$\Delta P_o \times 10^{-5}$ (Pa)	$\overline{\Delta P} \times 10^{-5}$ (Pa)	$\overline{J}_w \times 10^6$ ($m^3/(m^2 s)$)
0.3	0.29953	0.29977	2.358
0.5	0.49953	0.49977	3.472
0.8	0.79953	0.79977	4.684
1.1	1.09953	1.09977	5.913
1.4	1.39953	1.39977	6.517

The feed solution temperature in all experiments was kept at 25°C by a thermostat. During a run both the permeate and the retentate were recycled back to the feed tank. The experimental procedure was as follows. First, a fresh tubular-membrane module was used to measure the permeate fluxes of pure-water ultrafiltration J_w, for determining the intrinsic resistance of the membrane. Next, the steady permeate fluxes of liquid solution at the ten outlets, $z_j = [2 + 4(j-1)] \times 10^{-2}\ m$, $j = 1 \sim 10$, were measured under various C_i, Q_i, and ΔP_i. After each experimental run, the membrane was cleaned by the methods of high circulation and backflushing with 10% NaOH solution, 10% HNO_3 solution, and water. The cleaning procedure was repeated until the original water flux has been restored.

TABLE 3
Experimental data for R_f and ϕ

C_i (wt%)	$Q_i \times 10^6$ (m^3/s)	$(R_m + R_f) \times 10^{-10}$ ($Pa \cdot s/m$)	$R_f \times 10^{-10}$ ($Pa \cdot s/m$)	$\phi \times 10^{-5}$ (s/m)
0.1	1.67	1.8154	0.7662	1.738
	2.50	1.6219	0.5727	1.489
	3.33	1.4449	0.3957	1.296
	4.17	1.2773	0.2281	1.251
0.5	1.67	2.1702	1.1210	4.668
	2.50	2.0709	1.0217	4.317
	3.33	1.8873	0.8381	3.751
	4.17	1.7878	0.7386	3.328
1.0	1.67	2.5473	1.4981	5.918
	2.50	2.3691	1.3199	5.617
	3.33	2.1779	1.1287	4.851
	4.17	2.0477	0.9985	3.893

Many experimental data were obtained and some of them are listed in Tables 1–5.

Determination of R_m and R_f

The experimental data of the average permeate fluxes for pure water $(\overline{J}_w)_{exp}$ and solution $(\overline{J})_{exp}$ are presented in Tables 1 and 2, respectively. With the use of Table 1, a straight line of $(1/\overline{J}_w)_{exp}$ versus $(1/\overline{\Delta P})_{exp}$ could be constructed by the least-square method. Thus, the intrinsic

TABLE 2
Experimental data of average permeate flux for dextran T500 aqueous solution

	$Q_i \times 10^6 = 1.67\ m^3/s$		$Q_i \times 10^6 = 2.50\ m^3/s$		$Q_i \times 10^6 = 3.33\ m^3/s$		$Q_i \times 10^6 = 4.17\ m^3/s$	
C_i (wt%)	$\overline{\Delta P} \times 10^{-5}$ (Pa)	$\overline{J} \times 10^6$ ($m^3/m^2 \cdot s$)	$\overline{\Delta P} \times 10^{-5}$ (Pa)	$\overline{J} \times 10^6$ ($m^3/m^2 \cdot s$)	$\overline{\Delta P} \times 10^{-5}$ (Pa)	$\overline{J} \times 10^6$ ($m^3/m^2 \cdot s$)	$\overline{\Delta P} \times 10^{-5}$ (Pa)	$\overline{J} \times 10^6$ ($m^3/m^2 \cdot s$)
0.1	0.296	1.2372	0.302	1.3972	0.303	1.5757	0.308	1.7496
	0.504	1.8288	0.507	2.0748	0.492	2.3458	0.487	2.5814
	0.805	2.4722	0.792	2.8172	0.805	3.1927	0.801	3.4792
	1.093	2.9387	1.096	3.3594	1.112	3.8139	1.109	4.1268
	1.407	3.2828	1.393	3.7646	1.403	4.2798	1.382	4.6065
0.5	0.293	0.8161	0.295	0.8654	0.283	0.9664	0.296	1.0442
	0.492	1.0959	0.493	1.1669	0.489	1.3112	0.496	1.4288
	0.814	1.3463	0.805	1.4391	0.793	1.6261	0.806	1.7858
	1.082	1.5011	1.103	1.6084	1.105	1.8238	1.093	2.0127
	1.393	1.6056	1.409	1.7216	1.386	1.9569	1.409	2.1667
1.0	0.294	0.6733	0.291	0.7195	0.288	0.8024	0.302	0.9046
	0.497	0.9027	0.498	0.9542	0.495	1.0726	0.508	1.2354
	0.793	1.0903	0.792	1.1591	0.806	1.3126	0.802	1.5436
	1.108	1.2104	1.112	1.2834	1.108	1.4602	1.098	1.7279
	1.386	1.2868	1.385	1.3654	1.417	1.5578	1.384	1.8624

TABLE 4
The fitting parameter of experimental data for $C_i = 0.1$ wt% and $Q_i = 1.67 \times 10^{-6}\,m^3/s$

		$\Delta P_i = 0.3 \times 10^5$ Pa			$\Delta P_i = 1.4 \times 10^5$ Pa		
$z \times 10^2$ (m)	$\beta \times 10^{-5}$ (s/m)	$\Delta P \times 10^{-5}$ (Pa)	$J \times 10^6$ (m/s)	$\beta\Delta P(=R_p) \times 10^{-10}$ (Pa s/m)	$\Delta P \times 10^{-5}$ (Pa)	$J \times 10^6$ (m/s)	$\beta\Delta P(=R_p) \times 10^{-10}$ (Pa s/m)
2	1.6736	0.2999	1.2969	0.5019	1.4000	3.3516	2.3430
6	1.6876	0.2996	1.2928	0.5056	1.3997	3.3474	2.3621
10	1.7174	0.2994	1.2841	0.5142	1.3995	3.3395	2.4035
14	1.7635	0.2991	1.2714	0.5275	1.3992	3.3233	2.4675
18	1.8342	0.2989	1.2528	0.5482	1.3990	3.2962	2.5660
22	1.9243	0.2986	1.2289	0.5746	1.3987	3.2693	2.6915
26	2.0032	0.2984	1.2082	0.5978	1.3985	3.2497	2.8015
30	2.0729	0.2981	1.1906	0.6179	1.3982	3.2319	2.8983
34	2.1181	0.2979	1.1801	0.6310	1.3980	3.2155	2.9611
38	2.1749	0.2976	1.1661	0.6473	1.3977	3.2031	3.0399

resistance of the membrane tube employed in this study can be determined from Table 1 by using the following equation which can be modified from Eq. (1) by setting $R_f = 0$ and $R_p = 0$ for pure-water ultrafiltration

$$\frac{1}{(\bar{J}_w)_{exp}} = \frac{R_m}{(\overline{\Delta P})_{exp}} \tag{28}$$

In the above equation the average transmembrane pressure may be estimated by taking the arithmetic mean, according to the linear function of Eq. (12) as

$$(\overline{\Delta P})_{exp} = \frac{1}{2}[(\Delta P_i)_{exp} + (\Delta P_o)_{exp}] \tag{29}$$

in which $(\Delta P_i)_{exp}$ and $(\Delta P_o)_{exp}$ are the experimental values of the inlet and the outlet transmembrane pressures. Under various Q_i and $(\overline{\Delta P})_{exp}$, the measured value of R_m for the membrane system employed in the present study was determined graphically in Fig. 2 as

$$R_m = 1.0492 \times 10^{10}\,Pa \cdot s/m \tag{30}$$

Furthermore, the experimental data obtained in ultrafiltration of an aqueous solution may be also applied to determine R_f by Eq. (1) coupled with the use of Eqs. (3) (5,6) as

$$(\bar{J})_{exp} = \frac{(\overline{\Delta P})_{exp}}{R_m + R_f + \overline{\beta(\Delta P)}_{exp}} \approx \frac{(\overline{\Delta P})_{exp}}{R_m + R_f + \phi(\overline{\Delta P})_{exp}}$$

TABLE 5
The fitting parameter of experimental data for $C_i = 1.0$ wt% and $Q_i = 4.17 \times 10^{-6}\,m^3/s$

		$\Delta P_i = 0.3 \times 10^5$ Pa			$\Delta P_i = 1.4 \times 10^5$ Pa		
$z \times 10^2$ (m)	$\beta \times 10^{-5}$ (s/m)	$\Delta P \times 10^{-5}$ (Pa)	$J \times 10^6$ (m/s)	$\beta\Delta P(=R_p) \times 10^{-10}$ (Pa s/m)	$\Delta P \times 10^{-5}$ (Pa)	$J \times 10^6$ (m/s)	$\beta\Delta P(=R_p) \times 10^{-10}$ (Pa s/m)
2	3.5602	0.2995	0.9681	1.0663	1.3996	1.9691	4.9829
6	3.6647	0.2986	0.9513	1.0943	1.3987	1.9588	5.1258
10	3.7323	0.2977	0.9438	1.1111	1.3978	1.9391	5.2170
14	3.8335	0.2968	0.9311	1.1378	1.3969	1.9175	5.3550
18	3.9788	0.2959	0.9135	1.1773	1.3960	1.8871	5.5544
22	4.1603	0.2950	0.8952	1.2273	1.3951	1.8387	5.8040
26	4.3905	0.2941	0.8683	1.2912	1.3942	1.8008	6.1212
30	4.4770	0.2931	0.8596	1.3122	1.3932	1.7826	6.2374
34	4.5055	0.2922	0.8579	1.3165	1.3923	1.7718	6.2730
38	4.5325	0.2913	0.8571	1.3203	1.3914	1.7583	6.3065

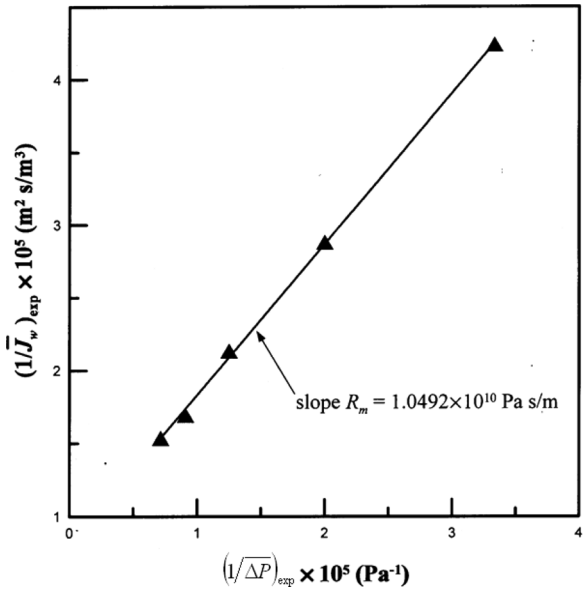

FIG. 2. A straight line of $(1/\bar{J}_w)_{exp}$ vs. $(1/\Delta P)_{exp}$.

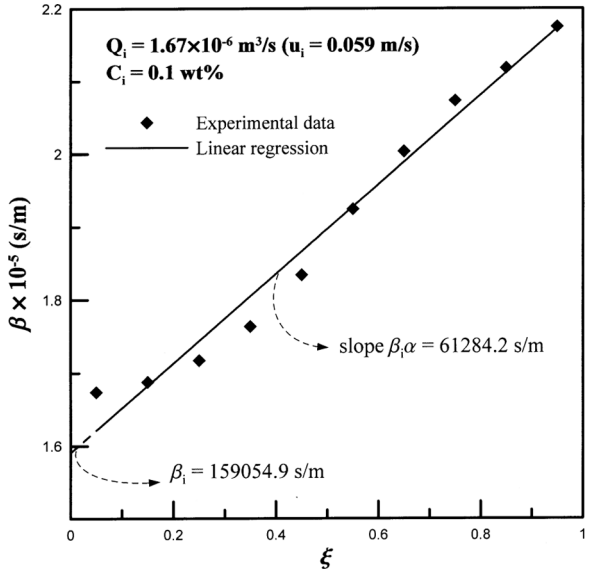

FIG. 3. A straight line of β vs. ξ.

or

$$\frac{1}{(\bar{J})_{exp}} = \phi + \frac{R_m + R_f}{(\overline{\Delta P})_{exp}} \tag{31}$$

Therefore, from a straight line plot of $(1/\bar{J})_{exp}$ versus $(1/\overline{\Delta P})_{exp}$, similar to Fig. 2, with the use of Table 2, the values of ϕ (the intersection at the ordinate) and $(R_m + R_f)$ (the slope), as well as R_f, were determined graphically. The results are given in Table 3 for various $u_i (= Q_i/\pi r_m^2)$ and C_i. Finally, the following correlation equations for ϕ and R_f were constructed as

$$\phi = 1.426 \times 10^5 \; u_i^{-0.39} C_i^{0.56} \tag{32}$$

$$R_f = 1.075 \times 10^9 \; u_i^{-0.73} C_i^{0.44} \tag{33}$$

Determination of β_i and α

Again, if the experimental data for the local permeate flux, J(z), in Tables 4 and 5 and transmembrane pressure, $\Delta P(z)$, are applied to Eq. (1) coupled with the use of Eq. (3), $R_p = \beta(z)\Delta P(z)$, then

$$\beta(z) = \frac{1}{[J(z)]_{exp}} - \frac{R_m + R_f}{[\Delta P(z)]_{exp}} \tag{34}$$

where, according to the linear decline of transmembrane pressure shown in Eq. (14)

$$[\Delta P(z)]_{exp} = (\Delta P_i)_{exp} - [(\Delta P_i)_{exp} - (\Delta P_o)_{exp}](z/L) \tag{35}$$

Some values of $\beta(z)$ obtained from Eq. (34) with known values of $(R_m + R_f)$, $[J(z)]_{exp}$ and $[\Delta P(z)]_{exp}$, are also listed in Tables 4 and 5. Therefore, from a straight-line plot of $\beta(\xi)$ versus ξ at a certain flow velocity u_i and feed concentration C_i, as shown in Fig. 3, the experimental values of β_i (the intersection at the ordinate) and $\beta_i\alpha$ (the slope) were determined graphically, according to Eq. (4). Finally, the correlation equations for β_i and α were constructed as

$$\beta_i = 3.54 \times 10^5 \; u_i^{-0.021} C_i^{0.373} \tag{36}$$

$$\alpha = 2.43 \times 10^{-3} \; u_i^{-1.666} C_i^{0.592} \tag{37}$$

RESULTS AND DISCUSSION

Comparison of Correlation Predictions with Experimental Results

The average values of the permeate flux $\bar{J}$ may be predicted from Eqs. (25)–(27) by the trial-and-error method coupled with the use of the correlation equations, Eqs. (30), (33), (36), and (37), and the system constants: $L = 0.4$ m, $r_m = 0.03$ m, and the fluid viscosity (21):

$$\mu = 0.894 \times 10^{-3} \exp(0.408 C_i) \; (Pa \cdot s) \tag{38}$$

Correlation predictions for $\bar{J}$ were thus calculated and some of the results are compared with the experimental data, as shown in Fig. 4. It is seen in this figure that the present model does not predict $\bar{J}$ well for higher transmembrane pressure.

The local values of the permeate flux $J(\xi)$ can be also predicted if the values of $\bar{J}$ thus obtained and above same

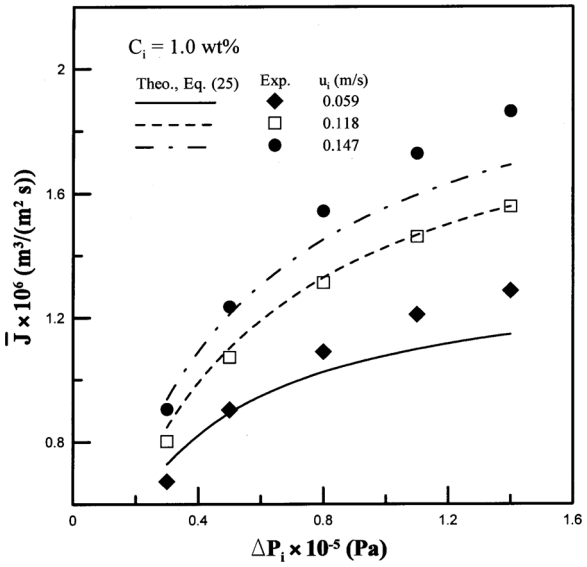

FIG. 4. Comparison of experimental results of $\bar{J}$ with correlation predictions for $C_i = 1.0$ wt%.

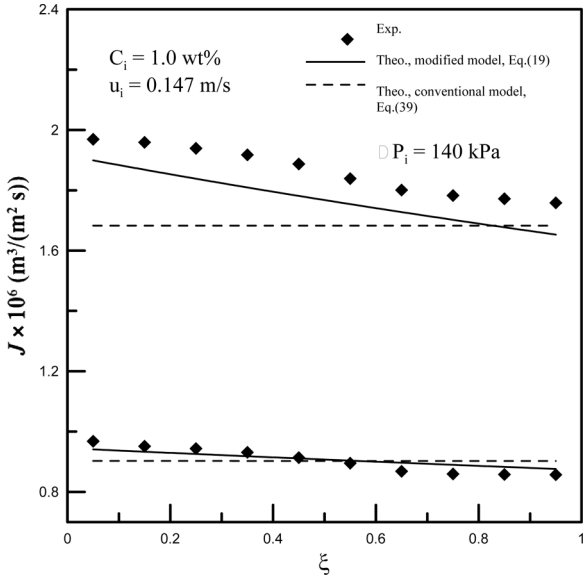

FIG. 6. Comparison of experimental results of J(z) with correlation predictions for $C_i = 1.0$ wt% and $u_i = 0.147$ m/s.

correlation equations and system constants are substituted into Eq. (19). Some prediction results are compared with the experimental results, as shown in Figs. 5 and 6. The prediction results for local permeate fluxes obtained from the traditional resistance-in-series model (5,6) with $\beta(\xi)$ replaced by a proportional constant, ϕ, were calculated by Eq. (1) coupled with the use of Eqs. (30), (32), and (33), and are also plotted in these figures. It is seen that the modified resistance-in-series model with the variable concentration-polarization resistance, $R_p = \beta_i(1 + \alpha\xi)\Delta P(\xi)$, is more precisely applicable than the conventional resistance-in-series model (5,6),

$$J(z) = \frac{\Delta P(z)}{R_m + R_f + \phi \Delta P(z)} \tag{39}$$

in which the term of concentration-polarization resistance, $R_p = \phi\Delta P(\xi)$, is nearly unchanged but slightly declined along the tube, as also shown in Figs. 7 and 8.

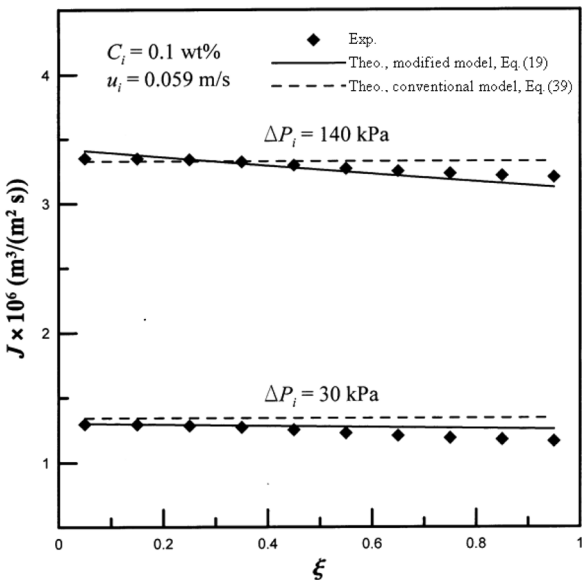

FIG. 5. Comparison of experimental results of J(z) with correlation predictions for $C_i = 0.1$ wt% and $u_i = 0.059$ m/s.

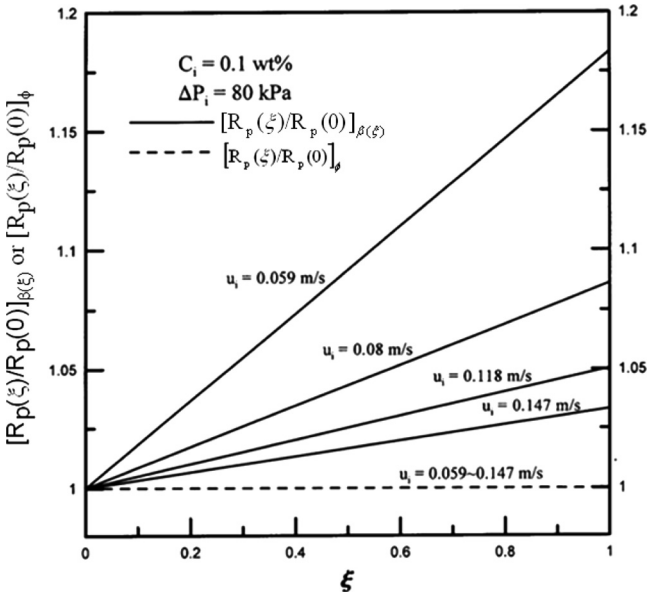

FIG. 7. Variation of concentration polarization along the tube for $C_i = 0.1$ wt% and $\Delta P_i = 80$ kPa.

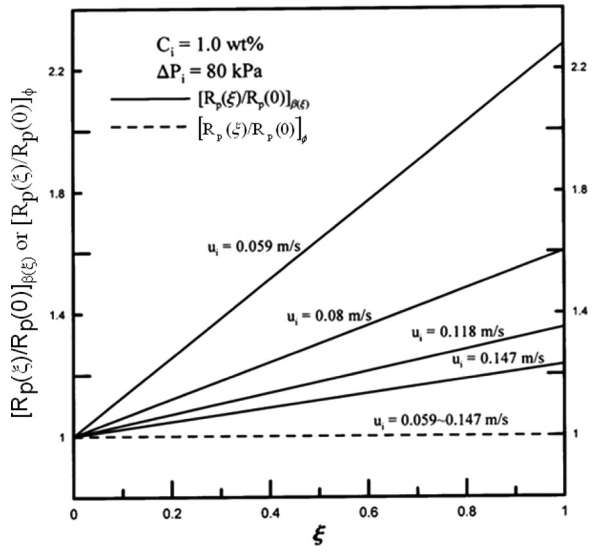

FIG. 8. Variation of concentration polarization along the tube for $C_i = 1.0$ wt% and $\Delta P_i = 80$ kPa.

Concentration Polarization Increment

The decline of the permeate flux along the cross-flow direction is mainly due to the decrease of transmembrane pressure $\Delta P(\xi)$ (driving force) and the increase of concentration polarization $R_p(\xi)$ (resistance). Figures 7 and 8 show the variations of $R_p(\xi)$ along the flow direction, with the traditional model defined in previous works (5,6), $\phi\Delta P(\xi)$, and with the modified model defined in present study, $\beta_i(1+\alpha\xi)\Delta P(\xi)$. It is obvious that the traditional model gives the incorrect description of $R_p(\xi)$, decreasing, instead of increasing, along the membrane tube. The correct definition of $R_p(\xi)$ by Eq. (5) does increase in the cross-flow direction, and the increment turns to more sensitive as the solution concentration increases or the fluid velocity decreases. The variations of concentration polarization may be also compared directly by the following expressions:

$$[R_p(\xi)/R_p(0)]_\phi = [\Delta P(\xi)/\Delta P_i] = 1 - (mQ_i - n\overline{J})(\xi/\Delta P_i) \tag{40}$$

$$[R_p(\xi)/R_p(0)]_{\beta(\xi)} = [(1+\alpha\xi)\Delta P(\xi)/\Delta P_i] = (1+\alpha\xi)[R_p(\xi)/R_p(0)]_\phi \tag{41}$$

CONCLUSION

The correlation equations, Eqs. (19) and (25), for predicting the local and average values of the permeate flux, respectively, in tubular-membrane ultrafilters, were derived from mass and momentum balances by the modified resistance-in-series model with the considerations of the increment of concentration polarization and the declines of transmembrane pressure and flow rate, along the membrane tube. The declines of the flow rate, transmembrane pressure, and permeate flux along the tube may be predicted from Eqs. (7), (14), and (19), respectively. For predicting the increment of concentration polarization, one may employ Eq. (5) coupled with the use of Eq. (14). Ultrafiltration of dextran T500 aqueous solution in a tubular microporous ceramic module has been carried out under various feed concentrations, transmembrane pressures, and feed flow rates. Correlation predictions are compared with the experimental results, as shown in Figs. 4–6. It is found that the correlation predictions of the local permeate flux obtained from the present modified resistance-in-series model are more accurate than those obtained from the conventional resistance-in-series model (5,6), in which the concentration-polarization resistance was described by an incorrect term, $\phi\Delta P(\xi)$, decreasing slightly along the tube, while in the present study, the increment of concentration polarization, $\beta_i(1+\alpha\xi)\Delta P(\xi)$, through the tube was taken into consideration, resulting in the correct decline of the permeate flux, as confirmed by the experiments. Therefore, the present model easily described the relationships of the decline of the permeate flux with operating and design parameters, and we believe that this model will also be suitable for most membrane ultrafiltration systems including systems with different kinds of feed solutions, different materials of membrane tubes, and various design and operating conditions.

ACKNOWLEDGEMENTS

The authors wish to express their thanks to the National Science Council of ROC for financial aid with Grant No. NSC 96-2221-E-032-033.

NOMENCLATURE

A, B, C	system constant, defined by Eq. (22), Eq. (23), Eq. (24) (Pa s/m)
C_i	concentration of feed solution (wt% dextran T500)
J	permeate flux of solution ($m^3/(m^2\,s)$)
L	effective length of membrane tube (m)
m, n	constant, defined by Eq. (16), Eq. (17) (Pa s/m^3)
P	pressure distribution on the tube side (Pa)
P_s	uniform permeate pressure on the shell side (Pa)
ΔP	transmembrane pressure, $P - P_s$ (Pa)
Q	volume flow rate in a tubular-membrane module (m^3/s)
r_m	inside radius of membrane tube (m)
R_f	resistance due to solute adsorption and fouling (Pa s/m)
R_m	intrinsic resistance of membrane (Pa s/m)
R_p	resistance due to concentration polarization (Pa s/m)
u	fluid velocity in the membrane tube, $Q/(\pi r_m^2)$ (m/s)

z axial coordinate (m)
z_j $j = 1, 2, \ldots, 10$, permeate fluxes exit at these ten points (m)

Greek Letters

α constant, defined in Eq. (4)
$\beta(z)$ linear function of z, defined in Eq. (4) (s/m)
ϕ constant defined by Eqs. (3) and (39) (s/m)
μ viscosity of solution (Pa s)
ξ dimensionless axial coordinate, z/L

Subscripts

i at the inlet
o at the outlet
w of pure water

Superscript

$-$ average value

REFERENCES

1. Porter, M.C. (1979) Membrane Filtration. In: *Handbook of Separation Techniques for Chemical Engineers*, Schweitzer, P.A., ed.; McGraw-Hill: New York, Sect. 2.1.
2. Cheryan, M. (1986) *Ultrafiltration Handbook*; Technomic Publishing Co.: Lancaster, PA, Sect. 8.
3. Cheryan, M.; Rajagopalan, N. (1998) Membrane processing of oily streams: Wastewater treatment and waste reduction. *J. Membr. Sci.*, 151: 13.
4. Fane, A.G. (1986) Ultrafiltration: Factors Influencing Flux and Rejection. In: *Progress in Filtration and Separation, Vol. 4*, Wakeman, R.J., ed.; Elsevier: Amsterdam.
5. Yeh, H.M.H.; Chen, Y.; Chen, K.T. (2000) Membrane ultrafiltration in a tubular module with a steel rod inserted concentrically for improved performance. *J. Membr. Sci.*, 168: 121.
6. Yeh, H.M.; Chen, K.T. (2000) Improvement of ultrafiltration performance in tubular membranes using a twisted wire-rod assembly. *J. Membr. Sci.*, 178: 43.
7. Thomas, D.C. (1967) Enhancement of forced convection heat transfer coefficient using detached turbulent promoters. *Ind. Eng. Chem. Proc. Des. Dev.*, 6: 385.
8. Peri, C.; Dunkley, W.L. (1971) Reverse osmosis of cottage cheese whey, Influence of flow conditions. *J. Food Sci.*, 36: 395.
9. Poyen, S.; Quemeneur, F.; Bariou, B. (1987) Improvement of the flux of permeate in ultrafiltration by turbulence promoters. *Int. Chem. Eng.*, 27: 441.
10. Howell, J.A.; Field, R.W.; Wu, D. (1993) Yeast cell microfiltration: Flux enhancement in baffled and pulsatile flow system. *J. Membr. Sci.*, 80: 59.
11. Gupta, B.B.; Wu, D.; Field, R.W.; Howell, J.A. (1994) Permeate Flux Enhancement Using a Baffle in Microfiltration with Mineral Membrane. In: *Separation Technology Vol. 11*, Vasant, E.F., ed.; Elsevier Science: BV, p. 559.
12. Gupta, B.B.; Howell, J.A.; Wu, D.; Field, R.W. (1995) A helical baffle for cross- flow microfiltration. *J. Membr. Sci.*, 99: 31.
13. Howell, J.A.; Field, R.W.; Wu, D. (1996) Ultrafiltration of high viscosity solution: Theoretical developments and experimental findings. *Chem. Eng. Sci.*, 51: 1405.
14. Da Costa, A.R.; Fane, A.G.; Fell, C.J.D.; Franker, A.C.M. (1991) Optimal channel spacer design for ultrafiltration. *J. Membr. Sci.*, 62: 275.
15. Da Costa, A.R.; Fane, A.G.; Wiley, D.E. (1994) Spacer characterization and pressure drop modeling in Spacer-filled channels for ultrafiltration. *J. Membr. Sci.*, 87: 79.
16. Da Costa, A.R.; Fane, A.G. (1994) Net-type spacers: Effect of configuration on fluid flow path and ultrafiltration flux. *Ind. Eng. Chem. Res.*, 33: 1845.
17. Field, R.W.; Wu, D.; Howell, J.A.; Gupta, B.B. (1995) Critical flux concept for microfiltration fouling. *J. Membr. Sci.*, 100: 259.
18. Fan, A.G. (1984) Ultrafiltration of suspensions. *J. Membr. Sci.*, 20: 249.
19. Nabetani, H.; Nakajima, M.; Watanabe, A.; Nakao, S.; Kumura, S. (1990) Effects of osmotic pressure and adsorption on ultrafiltration of ovalbumin. *AIChE J.*, 36: 907.
20. Chhatre, A.J.; Marathe, K.V. (2008) Modeling and performance study of MEUF of divalent metal ions in aqueous streams. *Sep. Sci. and Technol.*, 43: 3286.
21. Yeh, H.M.; Cheng, T.W. (1993) Resistance-in-series of membrane ultrafiltration in hollow fiber of tube-and-shell arrangement. *Sep. Sci. and Technol.*, 28: 1341.
22. Purkait, M.K.; DasGupta, S.; De, S. (2004) Resistance in series for micellar enhanced ultrafiltration of eosin dye. *Colloid and Interface Sci.*, 270: 496.
23. Rai, P.; Rai, C.; Majumder, G.C.; DasGupta, S.; De, S. (2006) Resistance in series model for ultrafiltration of mosambi (Citrus sinensis(L.) Osbeck) juice in a stirred continuous mode. *J. Membr. Sci.*, 283: 116.
24. Juang, R.S.; Chen, H.L.; Chen, Y.S. (2008) Resistance-in-series analysis in cross-flow ultrafiltration of fermentation broths of bacillus subtilis culture. *J. Membr. Sci.*, 323: 193.
25. Tansel, B.; Bao, W.Y.; Tansel, I.N. (2000) Characterization of fouling kinetics in ultrafiltration systems by resistances in series model. *Desalination*, 129: 7.
26. Derradji, A.F.; Taha, S.; Dorange, G. (2005) Application of the resistances in series model in ultrafiltration. *Desalination*, 184: 377.